VENTILATION TECHNOLOGIES IN URBAN AREAS

19TH ANNUAL AIVC CONFERENCE
OSLO, NORWAY, 28-30 SEPTEMBER 1998

SIMULATION OF INFILTRATION HEAT RECOVERY

C R Buchanan and M H Sherman

Energy Performance of Buildings Group
Indoor Environment Department
Environmental Energy Technologies Division
Lawrence Berkeley National Laboratory
University of California
USA

Simulation of Infiltration Heat Recovery

C. R. Buchanan and M. H. Sherman[1]
Energy Performance of Buildings Group
Indoor Environment Department
Environmental Energy Technologies Division
Lawrence Berkeley National Laboratory
University of California

Abstract

Infiltration has traditionally been assumed to affect the energy load of a building by an amount equal to the product of the infiltration flow rate and the enthalpy difference between inside and outside. Results from detailed computational fluid dynamics simulations of five wall geometries over a range of infiltration rates show that heat transfer between the infiltrating air and walls can be substantial, reducing the impact of infiltration. The classical method for determining the infiltration energy load was found to over-predict the amount by as much as 95 percent and by at least 10 percent. However, in order to achieve significant heat recovery flow paths which are unlikely in adventitious leakage are required.

Nomenclature

c_p = specific heat capacity of air (1006 J/kg K)
c_{ps} = specific heat capacity of insulation solid component (1006 J/kg K)
c_{pw} = specific heat capacity of wall sheathing (1200 J/kg K)
g = gravity (9.81 m/s^2)
k = air thermal conductivity (0.025 W/m K)
k_{eff} = effective thermal conductivity of insulation (0.025 W/m K)
k_s = thermal conductivity of insulation solid component (0.041 W/m K)
k_w = wall sheathing thermal conductivity (0.13 W/m K)
Q = total (conduction and convection) heat load (W)
Q_{inf} = energy load due to infiltration (W)
Q_o = pure conduction heat load (W)
m = infiltration mass flow rate (kg/s)
p = air pressure (Pa)
t = time (s)
T = temperature (K)
T_i = inside air temperature (298 K)
T_o = outside air temperature (274 K)
T_s = temperature of insulation solid component (K)
T_w = wall sheathing temperature (K)

[1] LBNL-42098:This work was supported by the Assistant Secretary for Energy Efficiency and Renewable Energy, Office of Building Technology of the U.S. Department of Energy under contract no. DE-AC03-76SF00098.

u = air flow velocity in x-direction (m/s)
v = air flow velocity in y-direction (m/s)
x = horizontal co-ordinate (m)
y = vertical co-ordinate (m)

α = insulation permeability (10^{-8} m^2)
$\Delta T = T_i - T_o$ (24 K)
ε = infiltration heat exchange effectiveness (dim)
ϕ = mass fraction of air in wall insulation material (0.99)
μ = air viscosity (1.72×10^{-5} kg/m s)
ρ = air density (kg/m^3)
ρ_s = density of insulation solid component (70 kg/m^3)
ρ_w = wall sheathing density (544 kg/m^3)

Introduction

Air leakage through building envelopes, infiltration, is a common phenomenon, which impacts both indoor air quality and building energy consumption. Some researchers have studied the potential of reducing building energy consumption by intentionally incorporating this process into the building design (3,9,15). In this technique, known as dynamic insulation, air is drawn through the building envelope in a direction that opposes the natural conductive flow of energy, so that some portion of the energy ordinarily lost to conduction is recovered.

In the general case, however, infiltration is unintentional and uncontrolled. Claridge and Bhattacharyya (7) note that a great deal of work has been devoted to the prediction and measurement of infiltration in building systems, but little effort has been directed toward determining the actual energy impact of infiltration. Infiltration can contribute a significant amount to the overall heating or cooling load of a building, but the actual size of the effect depends on a host of factors, including environmental conditions, building design, and construction quality. Based on experimental measurements taken at 50 residential buildings, Caffey (5) concluded that up to 40 percent of the heating/cooling costs in the homes studied was due to infiltration. In another study of residential buildings, Persily (13) attributed about one-third of the heating/cooling requirements to infiltration. Sherman and Matson (14) examined measured leakage data and concluded that a high fraction of the space conditioning load in U.S. buildings was due to infiltration. The results of a recent study (12) of U.S. office buildings performed by the National Institute of Standards and Technology (NIST) show that air leakage accounts for about 15 percent of the heating load in office buildings nationwide and about 1 or 2 percent of the cooling load. By all measures, the impact of infiltration can be sizeable and, so, should be considered in calculations of building energy consumption.

$$Q_{\text{inf}} = \dot{m} c_p (T_i - T_o) \quad (1)$$

The traditional method of accounting for the extra load due to infiltration is to simply add another term to the energy balance. The extra term, shown in equation 1, is the product of the infiltrating air mass flow rate, the specific heat capacity of air, and the temperature difference between inside and outside. Note this term does not include the effects of moisture in the air. This equation is appropriate if the leaking air does not interact themally with the

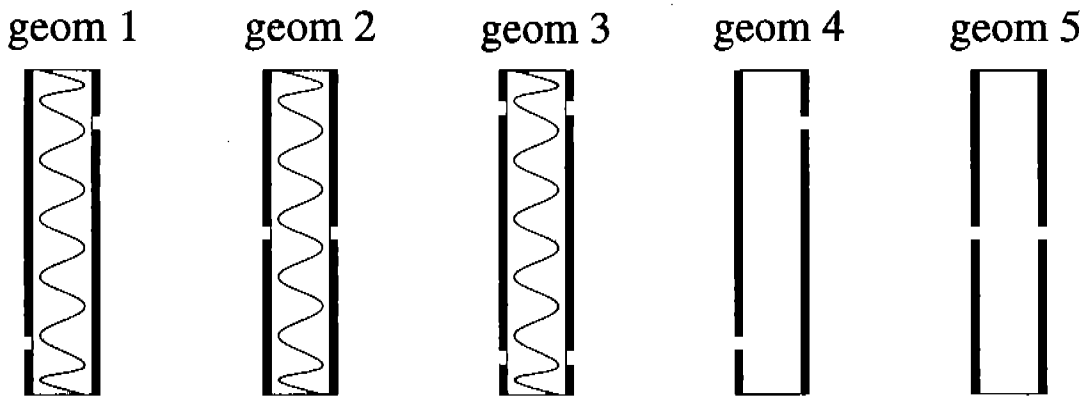

Figure 2: The five wall geometries examined; 1,2, & 3 are insulated and 4 & 5 are empty

Problem Formulation

The room represents a row-house inner unit (figure 1) and is composed of an infiltrating wall, a corresponding exfiltrating wall, and a ceiling, floor, front wall, and rear wall with no air leakage. The building envelope is separated into non-interacting wall elements, which are examined individually. Information from the individual walls is added together to determine the overall impact for a complete room system. The windward and leeward walls, both of the same geometry type, are matched by their air leakage rates and have crack lengths that extend the entire depth of the wall (10 m). The bulk air flow within the room is not represented, but this should not be a problem because, as Etheridge (8) notes, the internal room air flow has only a secondary effect on infiltration. The most important influences are wind-induced pressure differences and buoyancy of room air in the vicinity of the wall. Both are represented in these simulations.

The wall section is modeled as a two-dimensional, time-dependent system. Air flow and energy transport within the air are determined via the Navier-Stokes and energy equations (equations 2-5), respectively. A laminar representation is used for the flow. Solutions show this to be a reasonable assumption, as the Reynolds number at the crack under the highest pressure difference for the empty wall is only about 2000. Velocities elsewhere in the flow are much lower and would not provide the potential for turbulence. The plywood sheathing is represented as an impermeable, solid material. Energy transport within this material is calculated via the conduction equation (equation 6). Insulation in the wall is represented as a porous material. Air flow through the insulation is determined via Darcy's Law (equations 7 & 8), a common model for flow through porous media (4,10). Energy transport through the insulation is determined via a modified form of the energy equation (equation 9). In equation 9, an effective conductivity, given by equation 10, is used in the conduction flux term and the thermal inertia of the solid component is included in the transient term.

$$\frac{\partial \rho}{\partial t} + \frac{\partial \rho u}{\partial x} + \frac{\partial \rho v}{\partial y} = 0 \quad (2)$$

$$\frac{\partial \rho u}{\partial t}+\frac{\partial \rho u u}{\partial x}+\frac{\partial \rho u v}{\partial y}=-\frac{\partial p}{\partial x}+\mu\frac{\partial}{\partial x}\left[2\frac{\partial u}{\partial x}-\frac{2}{3}\left(\frac{\partial u}{\partial x}+\frac{\partial v}{\partial y}\right)\right]+\mu\frac{\partial}{\partial y}\left(\frac{\partial u}{\partial y}+\frac{\partial v}{\partial x}\right) \quad (3)$$

$$\frac{\partial \rho v}{\partial t}+\frac{\partial \rho u v}{\partial x}+\frac{\partial \rho v v}{\partial y}=-\frac{\partial p}{\partial y}+\rho g+\mu\frac{\partial}{\partial x}\left(\frac{\partial u}{\partial y}+\frac{\partial v}{\partial x}\right)+\mu\frac{\partial}{\partial y}\left[2\frac{\partial v}{\partial y}-\frac{2}{3}\left(\frac{\partial u}{\partial x}+\frac{\partial v}{\partial y}\right)\right] \quad (4)$$

$$c_p\frac{\partial \rho T}{\partial t}+c_p\frac{\partial \rho u T}{\partial x}+c_p\frac{\partial \rho v T}{\partial y}=k\frac{\partial^2 T}{\partial x^2}+k\frac{\partial^2 T}{\partial y^2}+\frac{\partial p}{\partial t}+u\frac{\partial p}{\partial x}+v\frac{\partial p}{\partial y} \quad (5)$$

$$\rho_w c_{pw}\frac{\partial T_w}{\partial t}=k_w\frac{\partial^2 T_w}{\partial x^2}+k_w\frac{\partial^2 T_w}{\partial y^2} \quad (6)$$

$$\frac{\partial p}{\partial x}=-\frac{\mu}{\alpha}u \quad (7) \quad , \quad \frac{\partial p}{\partial y}=-\frac{\mu}{\alpha}v \quad (8)$$

$$\frac{\partial}{\partial t}\left(\phi c_p \rho T+(1-\phi)c_{ps}\rho_s T_s\right)+c_p\frac{\partial \rho u T}{\partial x}+c_p\frac{\partial \rho v T}{\partial y}=k_{eff}\frac{\partial^2 T}{\partial x^2}+k_{eff}\frac{\partial^2 T}{\partial y^2}+\frac{\partial p}{\partial t}+u\frac{\partial p}{\partial x}+v\frac{\partial p}{\partial y} \quad (9)$$

$$k_{eff}=\phi k+(1-\phi)k_s \quad (10)$$

Thermal gradients in the system develop due to the difference between indoor and outdoor conditions giving rise to natural convection. As mentioned previously, it is important to represent the effects of buoyancy on the flow to properly determine infiltration rates and the heat flux at the wall, so buoyancy is included in these simulations. A simple, temperature-dependent empirical equation of state for the fluid density, coupled with the body force term in the fluid y-momentum equation introduces the effects of buoyancy into the flow.

Results and Discussion

Simulations are performed for the five wall geometries under wind-induced pressures ranging from 0.1-10 Pa with a constant temperature difference of 24K between inside and outside. Due to the complexity of the problem, it was not possible to achieve a converged solution using the steady-state equations. Therefore, the time-dependent equations were integrated in time until steady-state was reached. Comparison of results from simulations using a coarse computational grid (33,000 nodes) and a fine grid (140,000 nodes) for two different wall geometries showed that the coarse grid provided a grid-independent solution. All results presented here are steady-state solutions from simulations using a 33,000 node grid.

The main point of interest is the extra energy load introduced by infiltration. This is determined by first calculating the heat flux through the room walls with no air leakage, designated as Q_o. Then, the energy flux is determined for the same wall types with air leakage. The difference between the two values is the infiltration-induced energy load. The convection and conduction energy fluxes across the external (outside) face of each wall are

calculated for infiltrating and exfiltrating configurations. Using the external building face as the system control volume boundary is an arbitrary choice, the interior face could be used as well. However, it is important from an organizational standpoint that the energy accounting be performed at a consistent location.

For a given wall geometry, the infiltration air flow rate and energy flux vary with environmental conditions. The infiltration rate versus wind-induced pressure is shown in figure 3. In all cases, infiltration increases with wind pressure, but the actual values vary between geometries due to different flow resistances. The walls containing insulation (1-3) show a linear relationship between pressure and flow rate at pressures above about 0.5 Pa. This is the expected behavior, because the primary flow resistance in these cases, the insulation, is represented by linear flow-pressure relation, Darcy's Law. The empty walls (4-5) show a power law relationship with a flow exponent of about 0.5 at pressures above about 0.5 Pa. The literature (1,8,11) shows that for typical residential dwellings flow exponents range between one half to three quarters with averages typically about two-thirds. Although exponents up to unity are possible, they rarely play a significant role in adventitious leakage.

Below 0.5 Pa, the influence of the stack-induced pressure is comparable to that of the wind-induced pressure. It is interesting to note that for geometry 3, there is a low pressure plateau induced by the stack effect and leak geometry.

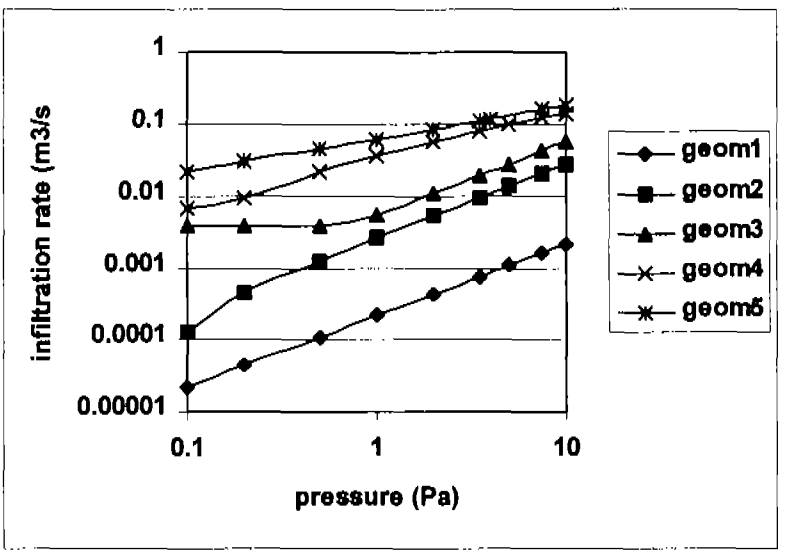

Figure 3: Infiltration rate vs. wind-induced pressure (ΔT=24K, crack length=10 m).

The extra energy load due to infiltration is given as a fraction of the classical load. The extra load, calculated via equation 11, uses the infiltration heat exchange effectiveness, ε, a non-dimensional factor introduced by Claridge (2,6,7), given in equation 12.

$$Q_{\inf} = (1-\varepsilon)\dot{m}c_p(T_i - T_o) \quad (11)$$

$$\varepsilon = 1 - \frac{Q - Q_o}{\dot{m}c_p \Delta T} \quad (12)$$

Figure 4 shows ε for the five wall geometries at various wind-induced pressures. In all cases, the heat recovery decreases with increasing flow rate. This is true for a given wall

geometry over the range of pressures or in a comparison of different wall geometries at a given pressure. The heat transfer becomes less efficient at high flow rates because there is less time for energy to be transported from the walls to the infiltrating air and less conducting energy available to recover.

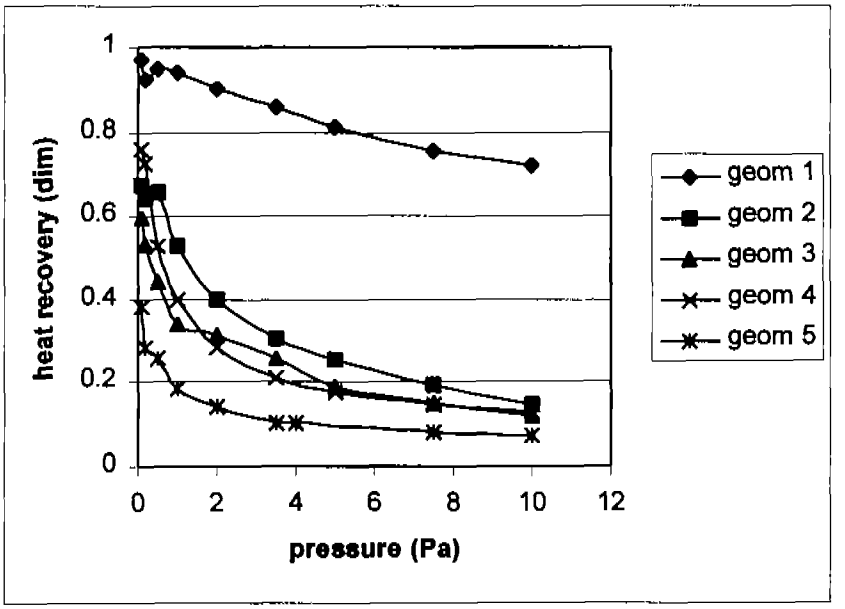

Figure 4: Heat recovery vs. wind-induced pressure for the five walls (ΔT=24 K).

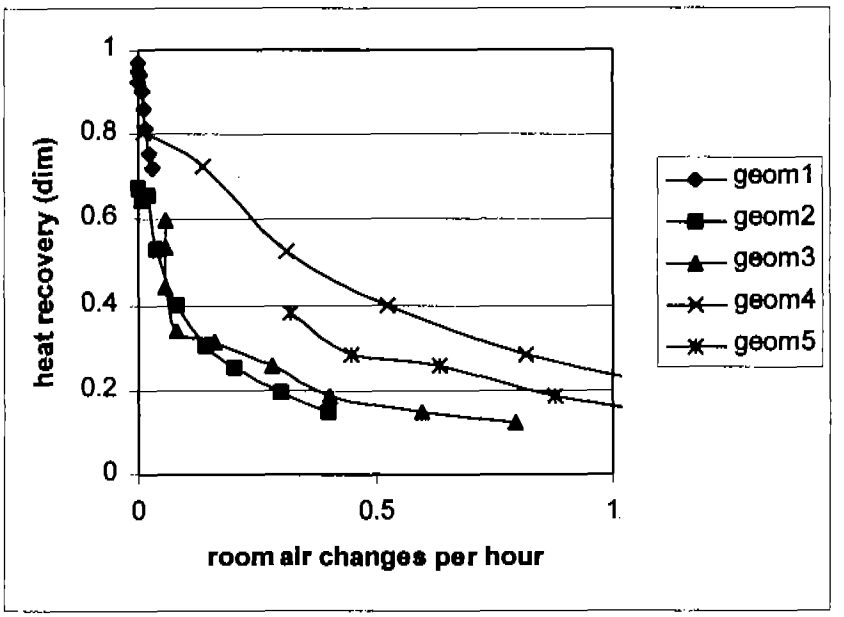

Figure 5: Heat recovery vs. infiltration rate in ACH.

Figure 5 shows that for a given infiltration rate (expressed here in room air changes) and wall type, insulated or empty, the heat recovery increases with infiltration path length. For example, wall geometries 4 and 5 are empty walls with long and short air flow paths, respectively. At a given infiltration rate the configuration with the long air flow path, geometry 4, has a higher heat recovery. Again, the increased heat recovery is due to longer

transit times for infiltrating air in the wall. The same trend is true for geometries 1 and 2, but is more difficult to see on the graph. It is interesting to note that the three insulated walls all seem to fall on a common curve, suggesting that a scaling law may apply. Future work on other configurations and geometries will be needed to explore this notion further.

An interesting point is revealed in comparison of geometries 2 and 3. Note that geometry 3 is similar to 2, except there are two holes instead of one. At pressures above about 0.5 Pa, geometry 3 has twice the flow as geometry 2, but nearly the same heat recovery. This indicates that in geometry 3 there is little interaction between the two holes, which is due to the large flow resistance of the insulation separating them. A wall of this design may not need to be modeled in its entirety. However, preliminary studies of this wall with an empty cavity show that there is a significant amount of interaction between the high and low holes, so this may not be a universal trait for all such wall designs.

In one sense, our results compare well to the experimental measurements of Claridge and Bhattacharyya (7). They calculated a maximum heat recovery of about 0.8 for a "diffuse" leakage path, which corresponds most closely to our geometry 1. This was nearly the average value determined in this study, as can be seen in figure 4.

In other ways, our results are not entirely comparable. In our simulations, we subjected each configuration to a range of pressures that are representative of the wind-induced pressures that real dwellings experience. For a given pressure, infiltration rates vary depending on the flow resistance (determined by the wall construction and environmental conditions), as can be seen in figures 3 and 5. In contrast, Claridge and Bhattacharyya adjusted the driving pressure to provide the same range of infiltration rates for each configuration. This technique is useful for some purposes, but the flow rates are too low to be representative of infiltration in most real dwellings, like our row-house scenario. When plotted against air change rate, all of their heat recovery values would be at very low air change rates, like our geometry 1 data. The infiltration rates for the configurations with "concentrated" leakage paths would be much higher (orders of magnitude) for realistic driving pressures.

Conclusions

Though still requiring substantiation, these results show the potential importance of infiltration heat recovery. In some circumstances, particularly in cases with low flow rates and long air flow paths, the heat recovery can be substantial, up to 95 percent. In these cases, the classical method will greatly over-predict the extra heating load due to infiltration. Even when the heat recovery is at the lowest level calculated, about 0.1, the classical method will over-predict the infiltration load by 10 percent. All leakage paths have not been represented in our simulations, but it seems that some modification should be considered to the classical method to increase its accuracy.

In reality, the importance of infiltration heat recovery will be determined by the particulars of the problem. For example, Sherman and Matson (14) found infiltration rates in typical U.S. housing stock to be around 1 ach. Our results suggest that about 10-20 percent of the heat would be recovered at these flow rates, so it is unlikely that this mechanism plays a large role in the rather leaky envelopes of U.S. housing stock. In new construction, where infiltration rates can be quite low, infiltration heat recovery could be a significant effect,

provided the infiltrating air goes through the insulating layers and not just directly through holes. However, this leakage scenario is associated with high flow exponents, which are not observed in most housing stock. Consequently, we would not expect this leakage scenario to occur, except in cases where it has been included in the design, as in dynamic insulation, and, so, the infiltration heat recovery would not be large.

The results in this report are limited to just a few test cases, but future work will include other wall geometries, more diverse environmental conditions, and integration of these findings into whole-building energy analysis models.

References

1) Baker, P. H., Sharples, S., Ward, I. C. (1987) "Air flow through cracks", *Building and Environment*, Vol. 22, No. 4, pp. 293-304.

2) Bhattacharyya, S., Claridge, D. E. (1995) "The energy impact of air leakage through insulated walls", *Transactions of the ASME,* Vol. 112, pp. 132-139.

3) Brunsell, J. T. (1995) "The indoor air quality and the ventilation performance of four occupied residential buildings with dynamic insulation", 16th AIVC Conference: Implementing the results of ventilation research, Palm Springs, USA, September 18-22, Proceedings Vol. 2, pp. 471-482.

4) Burns, P. J., Chow, L. C., Tien, C. L. (1977) "Convection in a vertical slot filled with porous insulation", *Int. J. Heat Mass Transfer*, Vol. 20, pp. 919-926.

5) Caffey, G. E. (1979) "Residential air infiltration", *ASHRAE Trans.*, Vol. 85, pp. 41-57.

6) Claridge, D. E., Liu, M. (1996) "The measured energy impact of infiltration in an outdoor test cell", *Transactions of the ASME*, Vol. 118, pp. 162-167.

7) Claridge, D. E., Bhattacharyya , S. (1990) "The measured impact of infiltration in a test cell", *J. Solar Energy Engineering*, Vol. 117, pp. 167-172.

8) Etheridge, D. W. (1988) "Modelling of air infiltration in single- and multi-cell buildings", *Energy and Buildings*, Vol. 10, pp. 185-192.

9) Jensen, L. (1993) "Energy impact of ventilation and dynamic insulation", 14th AIVC Conference: Energy impact of ventilation and air infiltration, Copenhagen, September 21-23, Proceedings, pp. 251-260.

10) Kohonen, R., Virtanen, M. (1987) "Thermal coupling of leakage flow and heating load of buildings", *ASHRAE Trans.*, Vol. 93, pp. 2303-2318.

11) Liddament, M. W. (1987) "Power law rules-- OK?", *Air Infiltration Review*, Vol. 8, No. 2, pp. 4-6.

12) "NIST estimates nationwide energy impact of air leakage in U. S. buildings" (1996) *J. Research of NIST*, Vol. 101, No. 3, p. 413.

13) Persily, A. (1982) "Understanding air infiltration in homes", Report PU/CEES No. 129, Princeton University Center for Energy and Environmental Studies, February, p. 335.

14) Sheman, M., Matson, N. (1993) "Ventilation-Energy liabilities in U.S. dwellings", 14th AVIC Conference: Energy impact of ventilation and air infiltration, Copenhagen, September 21-23, Proceedings, pp. 23-41.

15) Virtanen, M., Heimonen, I., Kohonen, R. (1992) "Application of the transfer function approach in the thermal analysis of dynamic wall structures", ASHRAE/DOE/BTECC Conference: Performance of the Exterior Envelopes of Buildings, December 7-10, Clearwater Beach, Florida, USA, Proceedings.